

The Effects of Inner- and Outer-Layer Turbulence in a Convective Boundary Layer on the Near-Neutral Inertial Sublayer Over an Urban-Like Surface

Marieta Cristina Castillo · Atsushi Inagaki · Manabu Kanda

Received: 25 March 2010 / Accepted: 1 April 2011
© Springer Science+Business Media B.V. 2011

Abstract A large-eddy simulation of the atmospheric boundary layer, large enough to contain both an urban surface layer and a convective mixed layer, was performed to investigate inner-layer and outer-layer scale motions. The objective was to determine the applicability of Monin–Obukhov similarity theory to inner-layer motions, to investigate the influence of outer-layer motions on surface-layer structure, as well as to assess the interaction of the two scales of motion. The urban surface roughness consisted of square-patterned cubic buildings of dimension H (40 m). A spatial filter was used to decompose the two scales in the inertial sublayer. The horizontal square filter of size $10H$ was effective in separating the inner-layer (surface-layer height $\approx 2H$) and outer-layer scales (boundary-layer height $\delta \approx 30H$), where the Reynolds stress contribution of the inner layer dominates in the logarithmic layer (depth $2H$). Similarity coefficients for velocity fluctuations were successfully determined for inner-layer motions in the surface layer, proving the robustness of Monin–Obukhov similarity for surface-layer turbulence. The inner-layer structures exhibit streaky structures that have similar streamwise length but narrower spanwise width relative to the streamwise velocity fluctuation field, consistent with observations from an outdoor scale model. The outer-layer motions to some extent influence the location of ejections and sweeps through updraft and downdraft motions, respectively, thus, disturbing the homogeneity and similarity of inner-layer motions. Although the horizontal averages of the variances and covariance of motions reveal that the Reynolds stresses are dominated by inner-layer structures, the localized influence of the interaction of outer-layer horizontal and inner-layer vertical motions on the Reynolds stress is not insignificant.

Keywords Atmospheric turbulence · Inertial sublayer · Inner-layer and outer-layer motions · Large-eddy simulation · Monin–Obukhov similarity · Reynolds stress

M. C. Castillo (✉) · A. Inagaki · M. Kanda
Department of International Development Engineering, Tokyo Institute of Technology, Tokyo, Japan
e-mail: criscastillo.ac.uk@gmail.com

1 Introduction

City dwellers have to contend with a number of problems related to urbanization such as urban heat island and air pollution. The increasing relevance and complexity of turbulence in the urban atmosphere have motivated scientists and engineers to focus on the city environment (e.g., Roth 2000; Cheng and Castro 2002; Kanda et al., 2004; Foster et al., 2006; Coceal et al., 2007; Inagaki and Kanda 2008, 2010). The bases for some of these studies are those concerning homogeneous surfaces that use similarity theories and models for turbulence structure. The challenge has been to modify and apply these simplified theories and models for complex, heterogeneous real world scenarios, such as pollution dispersion and heat ventilation in urban settings with massive roughness elements at very high Reynolds numbers that are not manageable by some research methods.

The similarity theory of Monin and Obukhov (1954) conjectured that any turbulence statistic in the atmospheric surface layer, normalised by an inner-layer scale parameter, is a function of the atmospheric stability parameter z'/L , where z' is the effective height (the difference between the elevation z and the zero-plane displacement d) and L is the Obukhov length:

$$L = - \frac{\overline{u_*^3} \langle \overline{\Theta} \rangle}{k g \langle \overline{w\theta_0} \rangle} . \quad (1)$$

Here, Θ is the potential temperature, k ($= 0.4$) is the von Karman constant, g ($= 9.81 \text{ m s}^{-2}$) is the acceleration due to gravity, $\langle \overline{w\theta_0} \rangle$ is the surface temperature flux, and u_* is the friction velocity, related to the surface shear stress through

$$u_* = (- \langle \overline{uw} \rangle_0)^{1/2} . \quad (2)$$

In the above, the angled brackets $\langle \rangle$ pertain to horizontal averaging, the overbar represents temporal averaging, and the terms z' and u_* are the inner-layer scaling parameters for length and velocity, respectively.

Various field experiments, as pioneered by the Kansas experiment (Businger et al., 1971; Wyngaard and Coté 1971), have both confirmed and contradicted the Monin-Obukhov similarity theory (MOST). The similarities of both wind shear and vertical velocity fluctuations have been confirmed for the atmospheric surface layer (Dyer 1974; Högström 1988). On the other hand, Kaimal et al. (1972, 1978) found that horizontal velocity fluctuations are not similar when normalised using inner-layer scaling, and that the low-frequency part of the horizontal velocity spectra is a function of δ/L , where δ is

the height of the convective boundary layer and an outer-layer scale for length (McNaughton and Brunet 2002).

Townsend (1961) and Bradshaw (1967) describe the nonconformity to MOST of the horizontal velocity fluctuations by decomposing turbulence in a turbulent boundary layer based on the contribution to the local Reynolds stress (i.e., active and inactive components). Townsend (1961) postulated that the active component of motion is responsible for the local Reynolds stress, follows inner-layer scaling, and is distinct from and does not interact with the outer-layer component. This outer-layer component, which was conjectured not to contribute to local Reynolds stress, has a scale of motion associated with the mixed layer, and follows outer-layer scaling.

The decomposition of inner-layer and outer-layer motions in the atmospheric surface layer was earlier attempted for coherent structures using eigenvector analysis (Mahrt and Gibson 1992), boundary-layer flows over gentle hills (Poggi and Katul 2008), and spectral data at the base of an advection inversion (McNaughton and Laubach 2000). The ‘brief-time-averaging’ used by McNaughton and Laubach (1998) was transformed into a ‘filter-space-averaging’ by Inagaki and Kanda (2010) to spatially filter the inner-layer motions in a comprehensive outdoor scale model (COSMO).

The concept of inactive motion has been debated and challenged (e.g., Högström and Bergström 1996; McNaughton and Brunet 2002; Morrison 2007; Zhao and Smits 2007), indicating a gap in Townsend’s hypothesis for explaining the non-similarity of horizontal fluctuations. Large outer-layer eddies are found to contribute to the Reynolds stress in the outer layer, and to the turbulent transfer of scalars such as heat (Antonia and Raupach 1993; Högström and Bergström 1996; Raupach et al., 1996; Bottema 1997; Högström et al., 2002). The turbulence models for a convective boundary layer of Hunt and Carloti (2001) and McNaughton (2004) were developed on the premise that the Reynolds stress in the convective outer layer affects that in the inner layer, thus invalidating Townsend’s concept of inactive motion. Results from experiments over a rice field (McNaughton and Brunet 2002) and fully-developed pipe flows (Morrison et al., 2002; Morrison 2007; Zhao and Smits 2007) have found evidence of the interaction between inner-layer and outer-layer turbulence, and that this interaction is nonlinear. In light of this, inner-layer and outer-layer motions are used to refer to the active and inactive motions, respectively (Laubach and McNaughton 2009).

The convective boundary layer can be divided into at least two main parts: the mixed layer, where large-scale convective mixing occurs and is capped by an inversion layer, and the underlying atmospheric surface layer, where surface shear is the dominant source for turbulence production. Within the atmospheric surface layer there is a

roughness sublayer, which lies over and is directly affected by the surface roughness and has three-dimensional flow characteristics (Rotach et al., 2005). If the ratio of the atmospheric boundary-layer height to the roughness element height, δ/H , is very large and the flow is fully turbulent with a sufficiently high Reynolds number (Jiménez 2004), an overlying inertial sublayer exists where the flow field is horizontally homogeneous, independent of the surface roughness except insofar as this affects the surface stress, and has a logarithmic velocity profile in neutral conditions. It is in this inertial sublayer where the maximum turbulence exchanges of momentum and scalars occur, and where inner-layer and outer-layer motions are said to co-exist.

There are two scales of organised structures corresponding to the inner-layer and outer-layer components of motion, respectively: low-speed streaks associated with Reynolds shear stress in the surface layer (Robinson 1991; Adrian et al., 2000), and streaky structures that are associated with thermal rolls in the convective boundary layer (Etling and Brown 1993). Over rough surfaces, the low-speed streaks in the urban setting (e.g., Kanda et al., 2004; Kanda 2006) and their integral length in the case of plant canopies (e.g., Kaimal and Finnigan 1994; Finnigan et al., 2009) scale to the size of the roughness elements. The thermal rolls consist of two-dimensional vortices that span relatively larger regions over longer periods. Both of these organised structures are responsible for the turbulent exchange of momentum and scalars between the surface and the atmosphere above, but the mechanics of generation of each of these structures are different. The interaction of these two structures (i.e., shear-driven streaks in the inner layer and thermal rolls at the outer layer) in the inertial sublayer is what has been referred to earlier (e.g., Hunt and Carlotti 2001; McNaughton 2004; McNaughton 2006; Laubach and McNaughton 2009).

The current paper follows McNaughton's (2004; see also Laubach and McNaughton 2009) concept of decomposing turbulence in the inertial sublayer into the inner-layer and outer-layer components, specifically the source of turbulence and scales of these components for convective boundary-layer flows: the inner-layer component is surface-shear driven with surface-layer scale while the outer-layer component is buoyancy driven with mixing-layer scale. Hunt and Carlotti (2001), Högström et al. (2002), and Drobinski et al. (2004), who extended Hunt and Morrison's (2000) turbulence model for neutral flows by theoretically applying it to convective boundary-layer flows, provide an alternative view wherein the outer eddies are composed of large-scale structures impinging onto the surface, including structures associated with thermal convection. As the outer eddies impinge onto the surface, their energy is passed onto smaller and smaller eddies through Richardson's energy cascade (Richardson 1920). For near-

neutral surface-layer flows, as outer convection weakens and surface shear strengthens, these outer eddies become less energetic (and the inner eddies more energetic) to the point that there is no room for an outer Richardson cascade to develop (Laubach and McNaughton 2009).

Various research methods have been used to describe the complex flows over urban environments: real city field campaigns (e. g., Rotach 1993; Roth 2000), outdoor scale models (Inagaki and Kanda 2008, 2010), wind-tunnel experiments (Cheng and Castro 2002; Hagishima et al., 2009), and numerical simulations (e.g., Kanda et al., 2004; Coceal et al., 2007; Xie et al., 2008; Bou-Zeid et al., 2009). Each research methodology has its own set of merits and faults, and it has been suggested that coupling two or more of these methods has the advantage of combining their capabilities and countering their weaknesses (Adrian 2002). Since computational fluid dynamics (CFD), specifically large-eddy simulation (LES), can explicitly resolve atmospheric flows of various scales ranging from an individual roughness element to an entire boundary layer (Kanda 2007), such technology is not limited by, and can validate the application of, building roughness models and the MOST applied for urban studies. The dimensionality, spatial resolution, and turbulence intensity that an LES model can handle are superior over most of the other methodologies, and sometimes compared to other CFD models, i.e., Reynolds-averaged Navier Stokes (RANS) and direct numerical simulation (DNS).

The objective of our large-eddy simulation study is to spatially decompose the inner-layer and outer-layer motions in the inertial sublayer of a near-neutral urban boundary layer, and to examine the similarity of inner-layer motions and the effect of outer-layer motions. The urban boundary layer modelled is composed of a fully developed mixed layer overlying an atmospheric surface layer with urban-like roughness. The contribution of the inner-layer and outer-layer motions to the local Reynolds stress and the interaction of the two scales are also calculated for the inertial sublayer. Our study follows Inagaki and Kanda's COSMO experiments (2008, 2010), which investigated the robustness of the MOST for a fully turbulent simplified city.

Similar CFD-based urban atmospheric studies used DNS (Coceal et al., 2007) and LES (Kanda et al., 2004; Xie et al., 2008; Bou-Zeid et al., 2009; Kono et al., 2010). These simulations had to compromise with the flow's Reynolds number, the size of the spatial domain or spatial resolution, due to computational resource limitations. It is imperative that the mixed-layer scale eddies be adequately modelled by increasing the vertical domain, that these outer-layer scale eddies be allowed to develop freely along an adequate horizontal domain, and that the smaller eddies be accurately resolved using a suitable spatial resolution. Relative to the above-mentioned numerical simulation

studies, the numerical domain used in our study has, by far, the largest spatial domain with an appropriate grid resolution for an atmospheric flow with very high Reynolds number.

2 Numerical Model

The atmospheric boundary layer, consisting of an urban surface layer and a convective mixed layer, was simulated. This was attained by initially setting a uniform streamwise velocity (20 m s^{-1}), constant heat flux for all horizontal surfaces (0.1 K m s^{-1}), and a typical daytime potential temperature vertical profile capped with a stable layer, approximating an entrainment layer near the top of the domain (Figs. 1 and 2). In order to appropriately study the influence of both inner-layer and outer-layer motions on the turbulence structure in the inertial sublayer, it is imperative that the domain is large enough to include both inner-layer scaled surface shear and outer-layer scaled convective mixing. The urban surface roughness consists of square-patterned cubic buildings of H size (40 m), with streamwise (x), spanwise (y), and vertical (z) domain volume of $64H$ by $64H$ by $65H$, respectively, a cube area density of 0.25, grid resolution of $H/16$ (2.5 m), and a total grid number of 1025 by 1025 by 562 along the x , y , and z axes. For the three-hour numerical simulation, all surfaces were non-slip, and the top boundary was set to slip. Cyclic condition was set for both horizontal domains; the volume flux of flow was conserved and not driven by an external pressure gradient or by the Coriolis Effect.

From the vertical profiles in Fig. 2, the effective vertical height of the atmospheric boundary layer is $\delta \approx 30H$ (i.e., height of inversion cap), and the logarithmic layer is at $H < z < 6H$. The stability of the atmospheric surface layer is near-neutral since the stability parameter z'/L is -0.03 at $z = 2H$, which is classified as near-neutral by the range of values ($|z'/L| \leq 0.05$) used by Roth (2000) and Inagaki and Kanda (2008). In the mixed layer ($3H < z < 30H$), the vertical profiles for potential temperature $\overline{\langle \theta \rangle}$, heat flux $\overline{\langle w\theta \rangle}$ and vertical velocity variance $\overline{\langle \sigma_w^2 \rangle}$ closely approximate the similarity relationships for a convective boundary layer (Stull 1988). The bulges at $z \leq H$ and $z \approx 1.75H$ for the vertical profile of $\overline{\langle \sigma_w^2 \rangle}$ are probably due to mixing within the urban canopy layer, and the maximum turbulent exchange between the roughness sublayer and inertial sublayer (Feigenwinter et al., 1999; Van Gorsel et al., 2003), respectively.

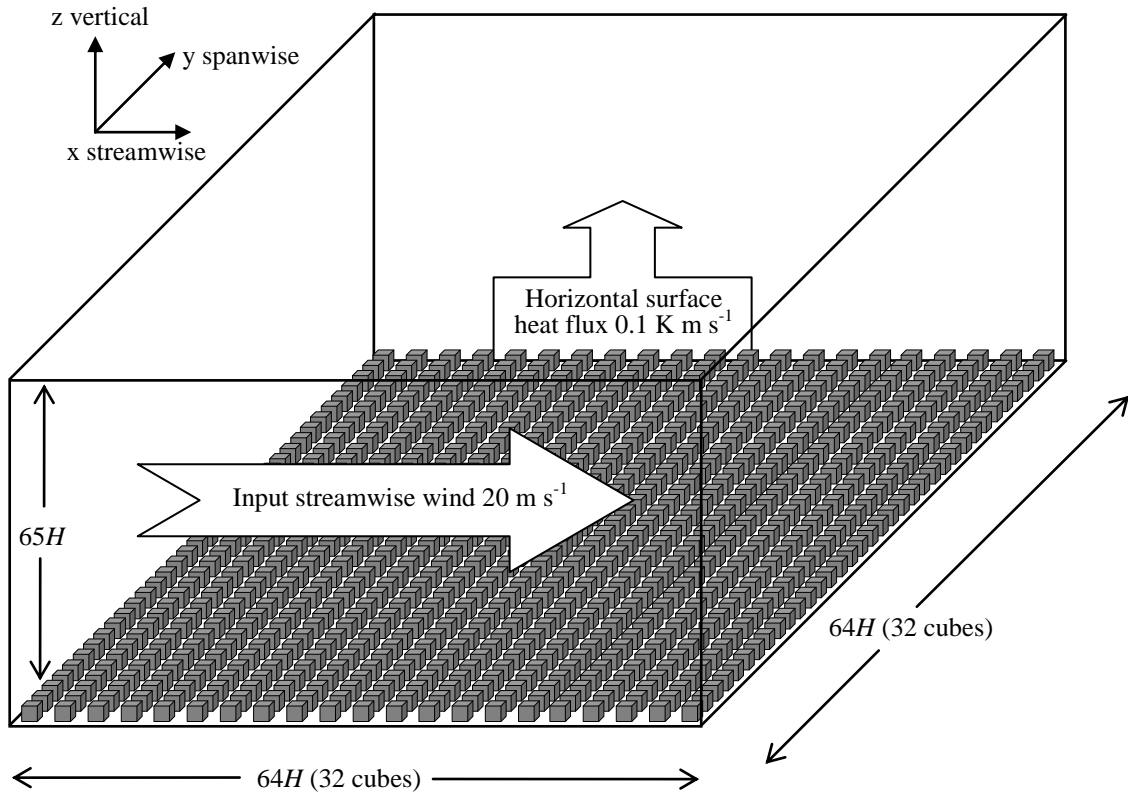


Figure 1. Schematic of the large-eddy simulation model domain.

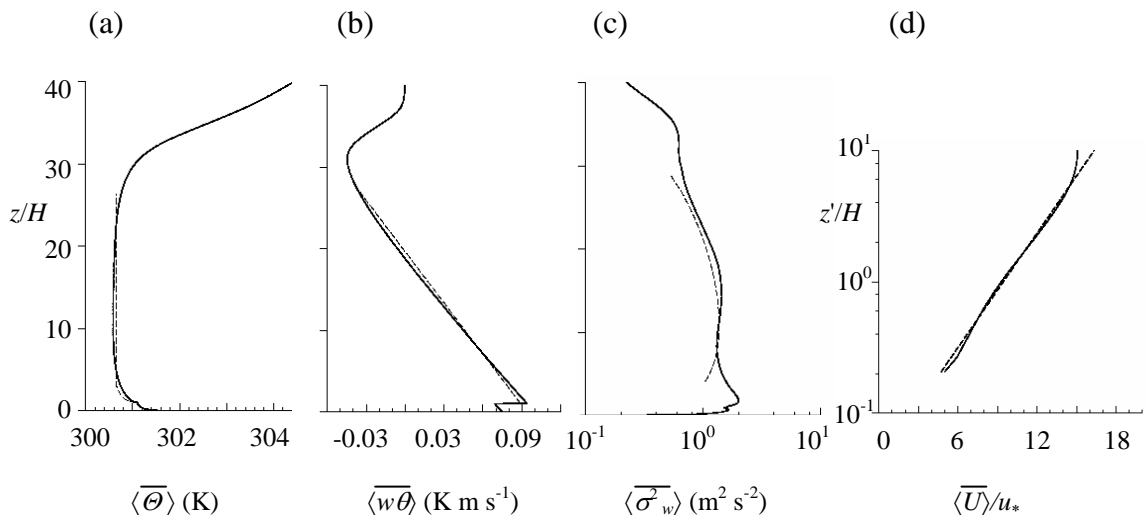


Figure 2. Vertical profiles for the large-eddy simulation model: (a) potential temperature $\langle \bar{\theta} \rangle$; (b) heat flux $\langle \overline{w\theta} \rangle$; (c) variance of vertical velocity $\langle \overline{\sigma_w^2} \rangle$; (d) logarithmic profile of the streamwise velocity normalised by friction velocity, $\langle \bar{U} \rangle / u_*$. Dashed lines are similarity relationships for neutral stability for the surface layer ($z \leq 3H$) and convective stability for the mixed layer ($0.1\delta \leq z \leq 0.9\delta$) (Stull 1988).

The urban version of the parallelised large-eddy simulation model (PALM) was used to solve the non-hydrostatic, incompressible Navier-Stokes equations in Boussinesq form, the first law of thermodynamics, and the equations for subgrid-scale turbulent kinetic energy (SGS-TKE) and scalar conservation (Letzel et al., 2008). Numerical schemes used were the second-order Piacsek-Williams-form C3 for advection and the third-order Runge-Kutta for time integration. The fractional step method ensures incompressibility, and the Temperton algorithm for fast Fourier transform (FFT) was used to solve for the resulting Poisson equation for perturbation pressure (Raasch and Schröter 2001). Implicit filtering of the governing equations follows the Schumann volume-balance approach, while turbulence closure for the LES was based on the modified Smagorinsky model, the flux gradient relationships of the 1/2th-order Deardorff scheme (Deardorff 1980). Turbulent diffusion coefficients for momentum and heat were parameterised by the SGS-TKE. Wall function was based on the MOST and prescribes a Prandtl-layer for each wall surface (Letzel 2007).

As a finite difference model, the parallelised large-eddy simulation model (PALM) stores variables on a staggered grid based on the Arakawa C grid, which doubles the effective spatial resolution. The mask method used in PALM to explicitly resolve solid obstacles on a rectangular grid, which was based on Kanda et al. (2004), proceeds as follows: numerical computation was executed at each grid point as if there were no obstacles; and forcing induced by physical boundary conditions were introduced to grid points corresponding to obstacle surfaces, wherein zero wall-normal velocities define wall positions (Letzel et al., 2008). The simplified and optimised mask method used in PALM reduces the three-dimensional obstacle into a two-dimensional topography, improving performance and minimising the computational load (Letzel 2007). To facilitate the onset of convection, random perturbations were initially imposed on the horizontal velocity field at every 150 seconds, which terminates when the perturbation energy (i.e., volume average of the TKE of the total model domain) exceeds a limit of $0.01 \text{ m}^2 \text{ s}^{-2}$. Rayleigh damping of a factor of 0.01 was applied near the top layer of the domain to dampen the gravity waves caused by convection that may spread vertically in the inversion layer and reflect at the top boundary (Raasch and Schröter 2001).

Instantaneous and one-hour averaged data fields of velocities (U , V , W) in the x , y , and z directions, as well as potential temperature, were collected from the final time interval of the three-hour simulation time. Most of the data analysis is done for the instantaneous fields, and temporal averaging, as represented by an overbar, is limited to flow statistics. The numerical simulation took approximately 600 hours real-time on 1024 CPUs on Sun FireTM X4600 clusters of the Tsubame, Tokyo Institute of

Technology's super grid computing system, using Message Passing Interface (MPI) for parallel communication.

3 Spatial Filtering

The concept of inner-layer and outer-layer flows refers to the origin of the respective eddies and is based on Townsend's hypothesis regarding active and inactive motions (Townsend 1976). For the numerical model of an urban convective boundary layer consisting of a shear-driven urban surface layer capped by a convective mixed layer, the inner-layer eddies originate from the urban surface layer and are created by surface shear, while the outer-layer eddies come from the convective mixed layer, similarly defined by Laubach and McNaughton (2009). McNaughton and Laubach (1998) used a 'brief-time-average' to separate the inner-layer and outer-layer scales, assuming that the spectral gap between the components was sufficiently divided by the temporal filter. Since the domain in our study is composed of instantaneous spatial data fields, instead of using temporal averaging as a high-pass filter (McNaughton and Laubach 1998), we follow Inagaki and Kanda's (2010) spatial decomposition for scale separation of the inner-layer and outer-layer components. In fact, Inagaki and Kanda (2010) found that spatial filtering is relatively more effective in preserving the inner-layer scale motion. Spatial filtering of the horizontal instantaneous motion u is used in order to distinguish between the inner-layer and outer-layer flows, following Inagaki and Kanda (2010):

$$u = u_{out} + u_{in} \quad , \quad (3)$$

$$u = [u] + u' \quad , \quad (4)$$

where the average of the fluctuation $[u]$ is the outer-layer component, the residual fluctuation u' is the inner-layer component, the square brackets $[]$ indicating averaging of the instantaneous flow field by spatial filtering for scale separation, and the prime ' for the corresponding spatial fluctuation. Using an *a posteriori* spatial filter for Eqs. 3 and 4, the outer-layer component u_{out} is the 'filter-space-average' $[u]$ at each grid point for a given elevation, while the inner-layer component u_{in} is the corresponding fluctuation u' from this average $[u]$. The same spatial filtering was also applied for vertical motion:

$$w = w_{out} + w_{in} \quad , \quad (5)$$

$$w = [w] + w' \quad . \quad (6)$$

The horizontal averages of the variances and the covariance of u and w are as follows:

$$\langle uu \rangle = \langle [u][u] \rangle + \langle u'u' \rangle + 2\langle [u]u' \rangle \quad , \quad (7)$$

$$\langle ww \rangle = \langle [w][w] \rangle + \langle w'w' \rangle + 2\langle [w]w' \rangle \quad , \quad (8)$$

$$\langle uw \rangle = \langle [u][w] \rangle + \langle u'w' \rangle + \langle [u]w' \rangle + \langle u'[w] \rangle \quad , \quad (9)$$

where the angled brackets represent horizontal averaging. Following the assumptions of Inagaki and Kanda (2008, 2010) for the inertial sublayer, where the outer-layer component does not contribute significantly to either vertical motion ($[w] \approx 0$) or momentum transfer ($[u][w] \approx 0$), and that inner-layer and outer-layer motions have insignificant interactions at high Reynolds number ($[u]w' \approx [u]u' \approx 0$), the variances and covariance of the horizontal and vertical velocities are given by:

$$\langle uu \rangle = \langle [u][u] \rangle + \langle u'u' \rangle \quad , \quad (10)$$

$$\langle ww \rangle = \langle w'w' \rangle \quad , \quad (11)$$

$$\langle uw \rangle = \langle u'w' \rangle \quad . \quad (12)$$

The terms in Eqs. 7-9 that are neglected in Eqs. 10-12 were investigated and are presented in Section 4.

As given by Eq. 12, it has been asserted that only the inner-layer component has a significant contribution to the surface-layer Reynolds stress (Townsend 1961). Thus, to determine the appropriate size for the spatial filter, the filter length must be between the two scales, and should yield a velocity flow field with ideally the same Reynolds stress as the original velocity field, or at least have the optimal contribution to the original Reynolds stress, i.e., $\langle u'w' \rangle / \langle uw \rangle$. For a given elevation z , the Reynolds stress of the filtered field is given by $\langle u'w' \rangle$, while that for the original field is $\langle uw \rangle$. For simplicity, the spatial filter is taken to be a horizontal square area. Based on the contribution of the filtered field to the local Reynolds stress with respect to the original velocity field (Fig. 3), a filter size of $10H$ was determined for $z \leq 2H$, with each contribution asymptoting closely to unity. The horizontally-averaged contribution of the filtered field at $z = 2H$ is approximately 95% of the original local Reynolds stress. For the $10H$ -size spatial filter,

the Reynolds stress contribution decreases significantly for $z > 2H$ since the influence of outer-layer turbulence gradually dominates as the distance from the surface roughness increases. In fact, Fig. 3 illustrates that the filter size for scale separation gradually increases with height, suggesting a continuum of turbulent scales between the smaller eddies in the inner layer and the larger ones in the outer layer.

Inagaki and Kanda (2010) used a linear spanwise filter and a temporal streamwise filter, the latter of which was converted to an equivalent linear filter by assuming frozen turbulent hypothesis. In Fig. 4, a linear filter along both directions for $z = 2H$ was also applied to the large-eddy simulation data. The linear spanwise filter closely approximates the values for the square filter, while the linear streamwise filter result in Reynolds stress contribution of only 60% of the square filter. This confirms the assertion of Inagaki and Kanda (2010) that linear filtering along the spanwise direction is relatively more effective in scale separation than along the streamwise direction.

The focus of the turbulence study is on $z = 2H$ since this is within the inertial sublayer. With a sufficient gap between the inner layer ($z = 2H$) and outer-layer scale ($\delta \approx 30H$) lengths, while a spatial filter size of $10H$ is between these two scales, the inner-layer and outer-layer scales can be effectively separated.

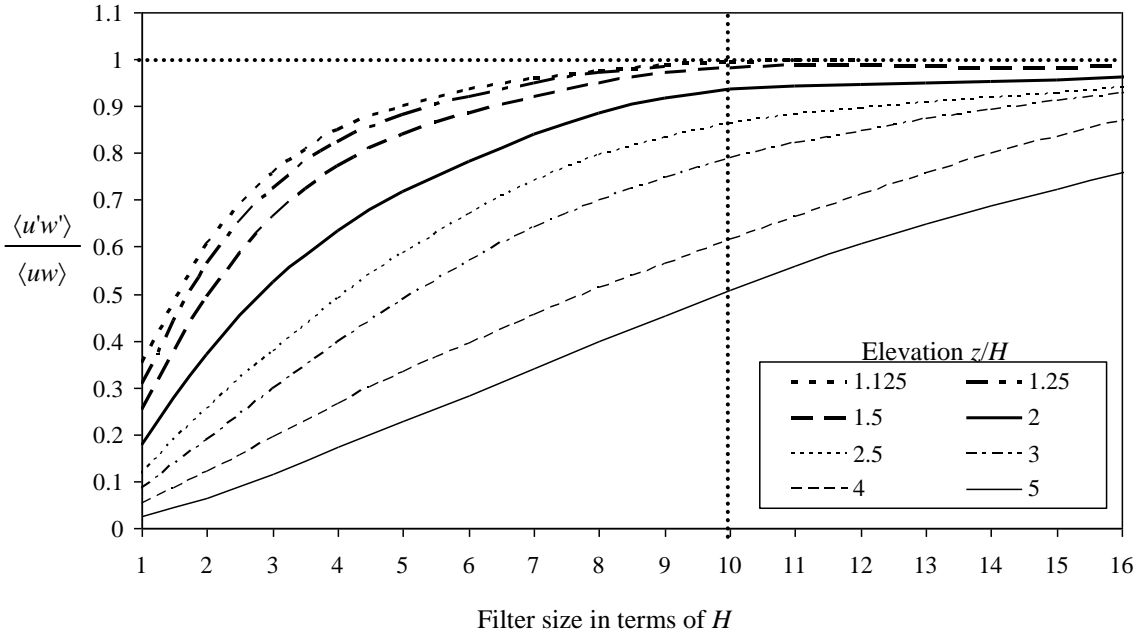


Figure 3. Reynolds stress contribution for $1.125H \leq z \leq 5H$ to determine the appropriate spatial filter size.

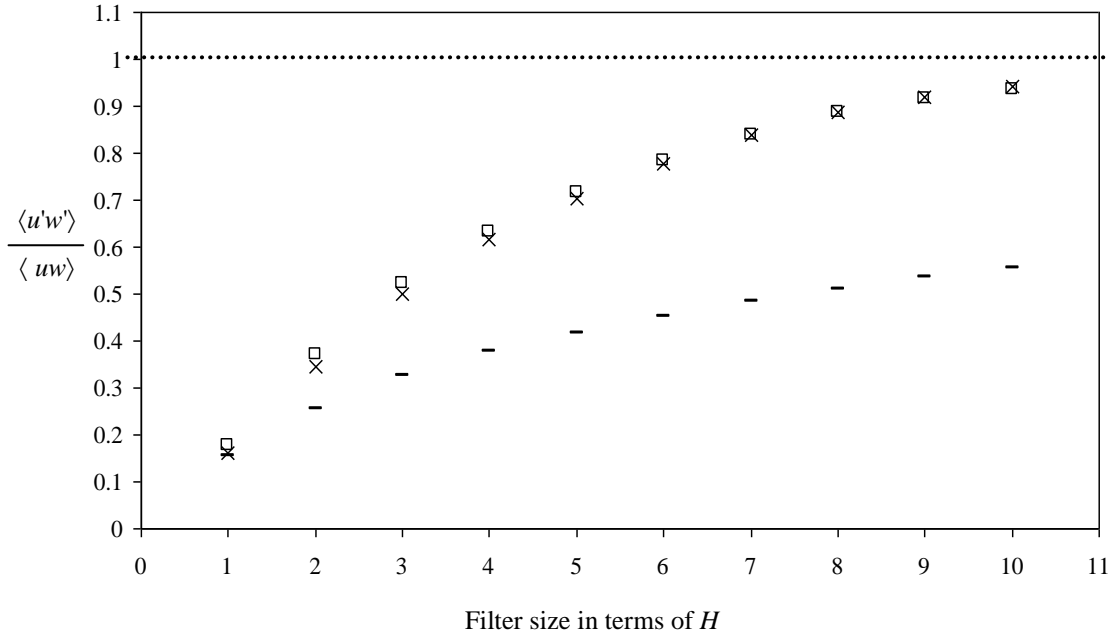


Figure 4. Reynolds stress contribution for $z = 2H$ using: — linear streamwise filter, × linear spanwise filter, and □ horizontal square filter.

4 Results and Analyses

Horizontal fields of instantaneous streamwise motions for $z = 2H$ are shown in Fig. 5, with the original u , inner-layer motion u' , and outer-layer motion $[u]$. These motions are subjected to conditional sampling by quadrant technique (Wallace et al., 1972; Willmarth and Lu 1972), where they are limited to ejections ($u < 0, w > 0$) and sweeps ($u > 0, w < 0$) for clarity in visualisation, justified by the fact that these two events are responsible for nearly all of the vertical turbulent exchange (Raupach 1981; Shaw et al., 1983; Finnigan 2000; Finnigan and Shaw 2000; Högström et al., 2002; Foster et al., 2006). The numerical results show ejections and sweeps each contributing at least 60% to the net Reynolds stress at $z = 2H$ across the whole domain, which is similar to a neutrally-stratified boundary layer over a sparse forest (Su et al., 1998), and slightly larger than the wind-tunnel results over urban-like roughness (Castro et al., 2006). Streamwise motions in Fig. 5 corresponding to ejections are clearly represented by negative values, while for sweeps by positive values.

The most noticeable aspects of the turbulence fields in Fig. 5 are that streaky structures are present in both fields of u and u' , while smooth, massive structures are present in the $[u]$ field. The streaky structures u and u' look quite similar, except that the

latter has narrower streaks than the former. This is consistent with the observations in the COSMO experiments, where u' structures are smaller along the spanwise direction, but have a comparable length with the u structures along the streamwise direction (Inagaki and Kanda 2010).

Upon close inspection of Fig. 5, the horizontal distribution of the ejections and sweeps for u' seem more homogeneous relative to u . This relative heterogeneity of u (Fig. 5a) is apparently the effect of outer-layer motion (Fig. 5c). Wherever positive structures dominate in Fig. 5c for $[u]$, the positive structures (i.e., sweeps) for the u field (Fig. 5a) are relatively larger than in the u' field (Fig. 5b). The same thing is true for the corresponding negative structures (e.g., ejections for Fig. 5a). Foster et al. (2006) interprets this as the effect of large-scale circulation being conducive for the formation of ejections in the upward flow, and sweeps in the downward flow.

It seems that ejections (i.e., upward flow) dominate the region defined by $0 < y/H < 32$, and sweeps (i.e., downward flow) for $32 < y/H < 64$ (see Fig. 5c). This is a consequence of the large-scale convective motion in the mixed layer, wherein the updraught motion dominates the region $0 < y/H < 32$, and the downdraught motion for $32 < y/H < 64$ (Stull 1988). From hereon, these will be referred to as the updraught and downdraught regions, respectively. The flow statistics for the half domains (Fig. 6) give evidence for these two regions. These updraught and downdraught motions referred here are of the mixed-layer scale that represents the outer-layer motions, the effects of which are present in the u field.

The flow statistics in Fig. 6 were temporally (i.e., final hour of simulation) and horizontally averaged based on their respective region, with the updraught and downdraught regions being half domains along the spanwise direction. The streamwise velocity of the downdraught region is relatively faster since this is directly from the mixed layer, while the streamwise velocity of the updraught region is dampened by the urban roughness. Although the momentum flux at the top of the urban roughness is approximately equal for both regions, the updraught region has a significantly larger momentum flux above the urban roughness. The large negative momentum flux in the mixed layer is caused by convective circulation (Stull 1988), wherein updraughts have been observed to have larger momentum flux for both neutral and convective boundary layers (Maitani and Shaw 1990; Moeng and Sullivan 1994). While the wind velocity for the total domain is the average of the two regions, the momentum flux, on the other hand, looks like the aggregate of the updraught and downdraught regions.

One criterion to test the validity of spatial filtering as a high-pass filter method for scale separation is the assumption that the inner-layer motion is wholly responsible for

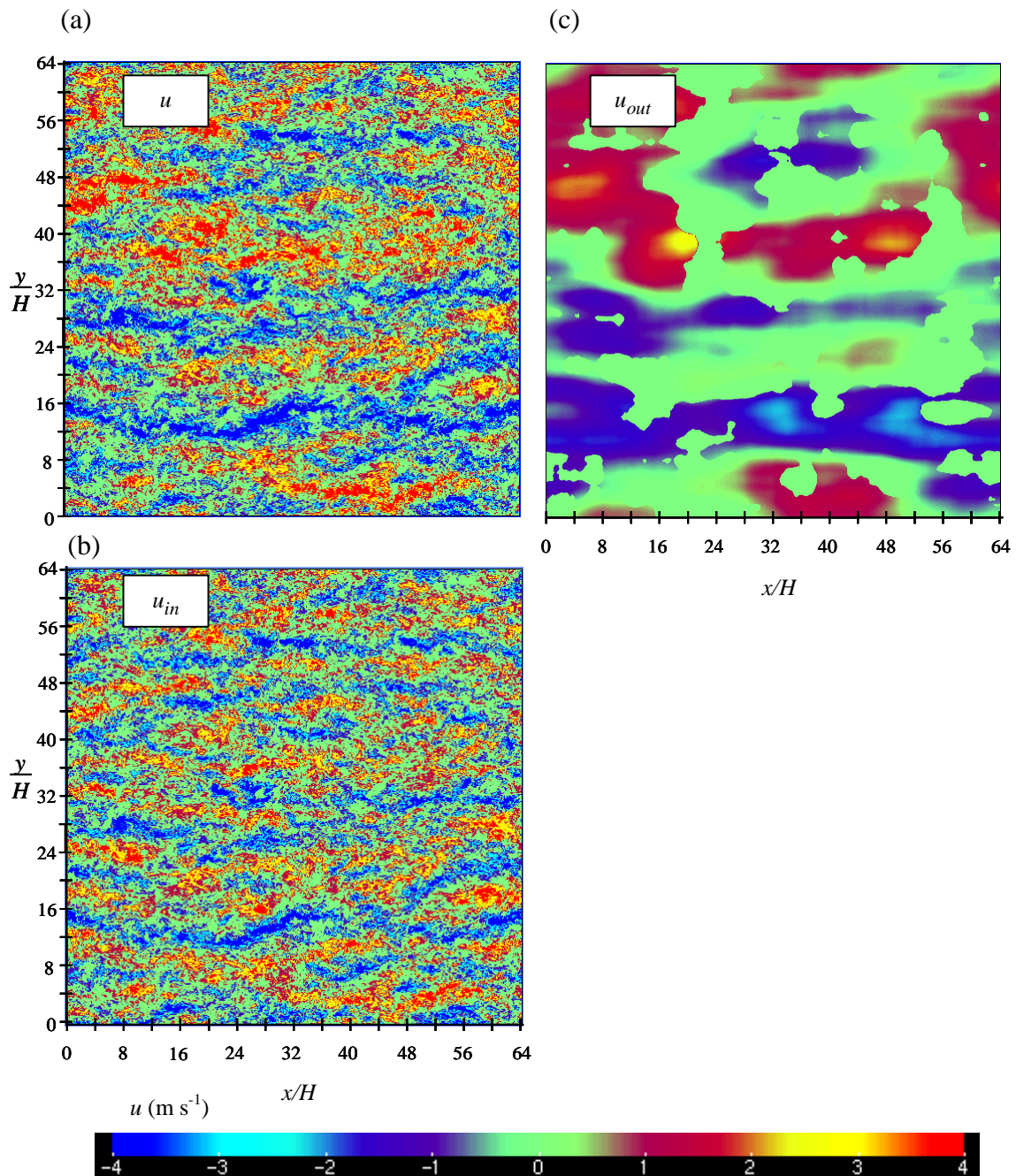


Figure 5. Horizontal instantaneous fields of streamwise velocity for $z = 2H$, which were conditionally sampled for ejections and sweeps: (a) u , (b) u' , and (c) $[u]$.

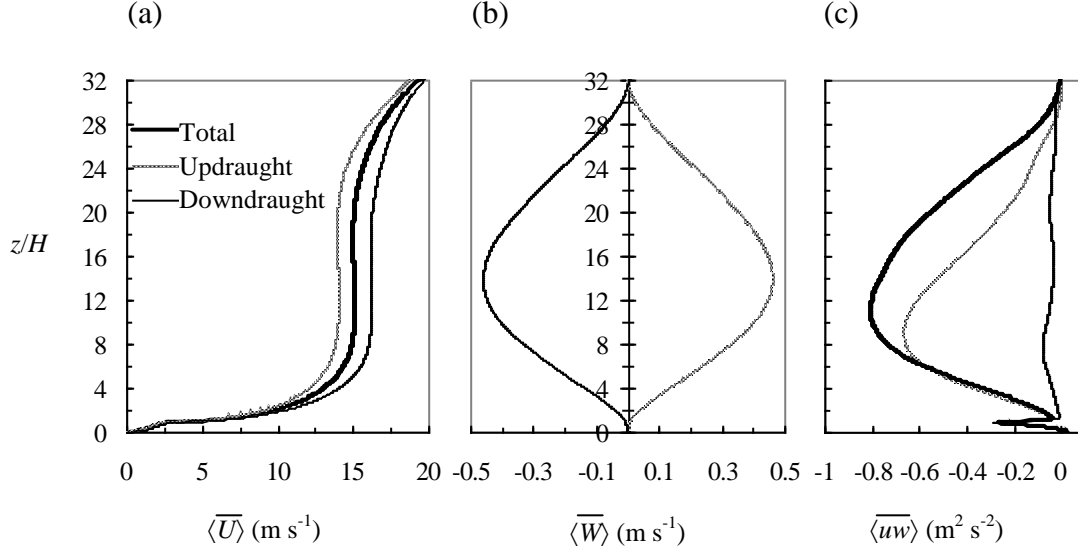


Figure 6. Horizontally- and temporally-averaged flow statistics for the entire domain, updraught and downdraught regions: (a) streamwise velocity $\langle \bar{U} \rangle$; (b) vertical velocity, $\langle \bar{W} \rangle$; (c) Reynolds stress, $\langle \bar{uw} \rangle$.

the surface-layer Reynolds stress. This assumption neglects the contribution of the outer layer and the interaction terms presented in Eq. 9, and will be tested in this section. Figure 7 presents the variance and covariance components in Eqs. 7-9 that are neglected in Eqs. 10-12, horizontal-averaged and normalised by their respective net values (i.e., from u and w), while Fig. 8 presents the horizontal distribution of all Reynolds stress components of Eq. 9 for $z = 2H$.

For $z \leq 2H$ (Fig. 7), as in Fig. 3, inner-layer motions dominate the variances and covariances with no significant contribution from the outer-layer scale and the interaction terms. As the vertical distance from the roughness elements increases, the outer-layer scale and interaction components slowly increase since outer-layer scale motion dominates the mixed layer. The interaction terms actually remain relatively insignificant even for $z > 2H$, and, together with the outer-layer component, $\langle [u][w] \rangle + \langle [u]w' \rangle + \langle u'[w] \rangle$ make up for the 5% residual shown in Fig. 3.

The Reynolds stress components for $z = 2H$, as presented in Fig. 8, have a sign convention based on that of the vertical component of motions, so that the positive and negative Reynolds stresses correspond to ejection- and sweep-induced values, respectively. The inner-layer scale covariance $u'w'$ (Fig. 8a) closely approximate the horizontal field of the original Reynolds stress uw (not shown here), which is consistent with the assumption that the surface-layer Reynolds stress is a consequence of inner-layer turbulence (Townsend 1976; Raupach et al., 1991). The structures representing the outer-layer scale $[u][w]$ and interaction terms $[u]w'$ and $u'[w]$ (Figs. 8b-d) are smaller

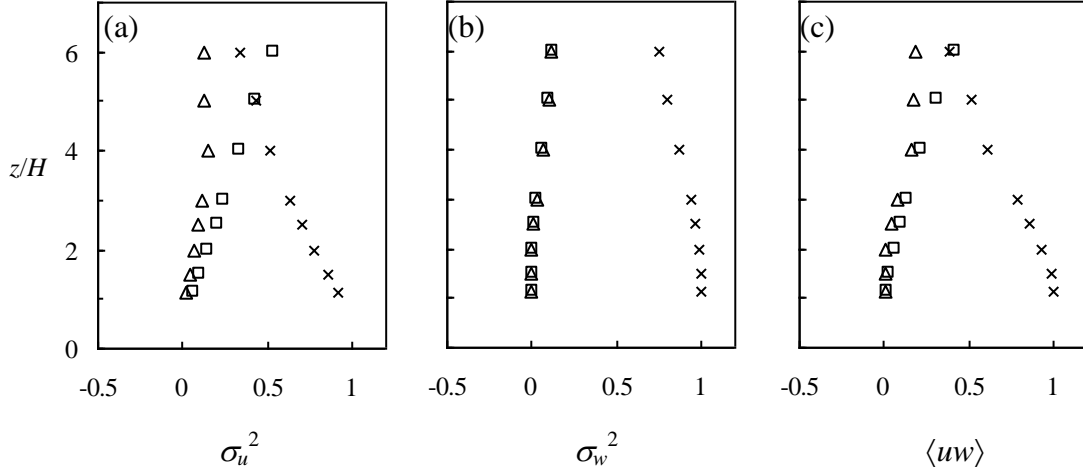


Figure 7 Normalised horizontal averages of variances and covariances of velocity components: (a) \times , $\langle u'u' \rangle / \langle uu \rangle$; \square , $\langle [u][u] \rangle / \langle uu \rangle$; \triangle , $2\langle [u]u' \rangle / \langle uu \rangle$; (b) \times , $\langle w'w' \rangle / \langle ww \rangle$; \square , $\langle [w][w] \rangle / \langle ww \rangle$; \triangle , $2\langle [w]w' \rangle / \langle ww \rangle$; (c) \times , $\langle u'w' \rangle / \langle uw \rangle$; \square , $\langle [u][w] \rangle / \langle uw \rangle$; \triangle , $\langle [u]w' \rangle + \langle u'[w] \rangle / \langle uw \rangle$.

than the $u'w'$ structures. Relative to $[u][w]$ and $u'[w]$, the streaky structures of $[u]w'$ are more prominent, with its pattern consistent with that of the $[u]$ structures in Fig. 5c. These localised $[u]w'$ streaks, along with their correspondence with Fig. 5c, suggest that the outer-layer motion, to a limited extent, influences the location of the ejections and sweeps in the logarithmic layer. Yet, Fig. 7c illustrates that $\langle [u][w] \rangle$ is comparable with $\langle [u]w' \rangle + \langle u'[w] \rangle$, clarifying that the positive and negative structures of $[u]w'$ (Fig. 8c) mostly cancel each other out in horizontal averaging as much as those for $[u][w]$ and $u'[w]$, resulting in the 5% residual in Fig. 3.

With the $u'w'$ structures closely approximating uw structures and the outer-layer scale and interaction terms having relatively small contribution to uw , the spatially-filtered motion appropriately represents the inner-layer component of motion that is responsible for most of the surface-layer Reynolds stress.

Figure 9 presents the normalised standard deviations of the velocity components σ_u/u_* , σ_v/u_* , and σ_w/u_* for the numerical simulation considering the u and u' fields. Friction velocity u_* , as defined in Eq. 2, is calculated from u and w at $z = 2H$. In the ordinate axis, $z' = z - d$, and z_0 is the surface roughness length, where $d \approx 0.9H$ and $z_0 \approx 0.03H$ based on the logarithmic velocity profile (Kaimal and Finnigan 1994). The results of the COSMO experiments of Inagaki and Kanda (2008, 2010), wind-tunnel experiments of Cheng and Castro (2002), and the compilation of Roth (2000) of urban experiments, are also included. The only other study that uses a similar linear filter to

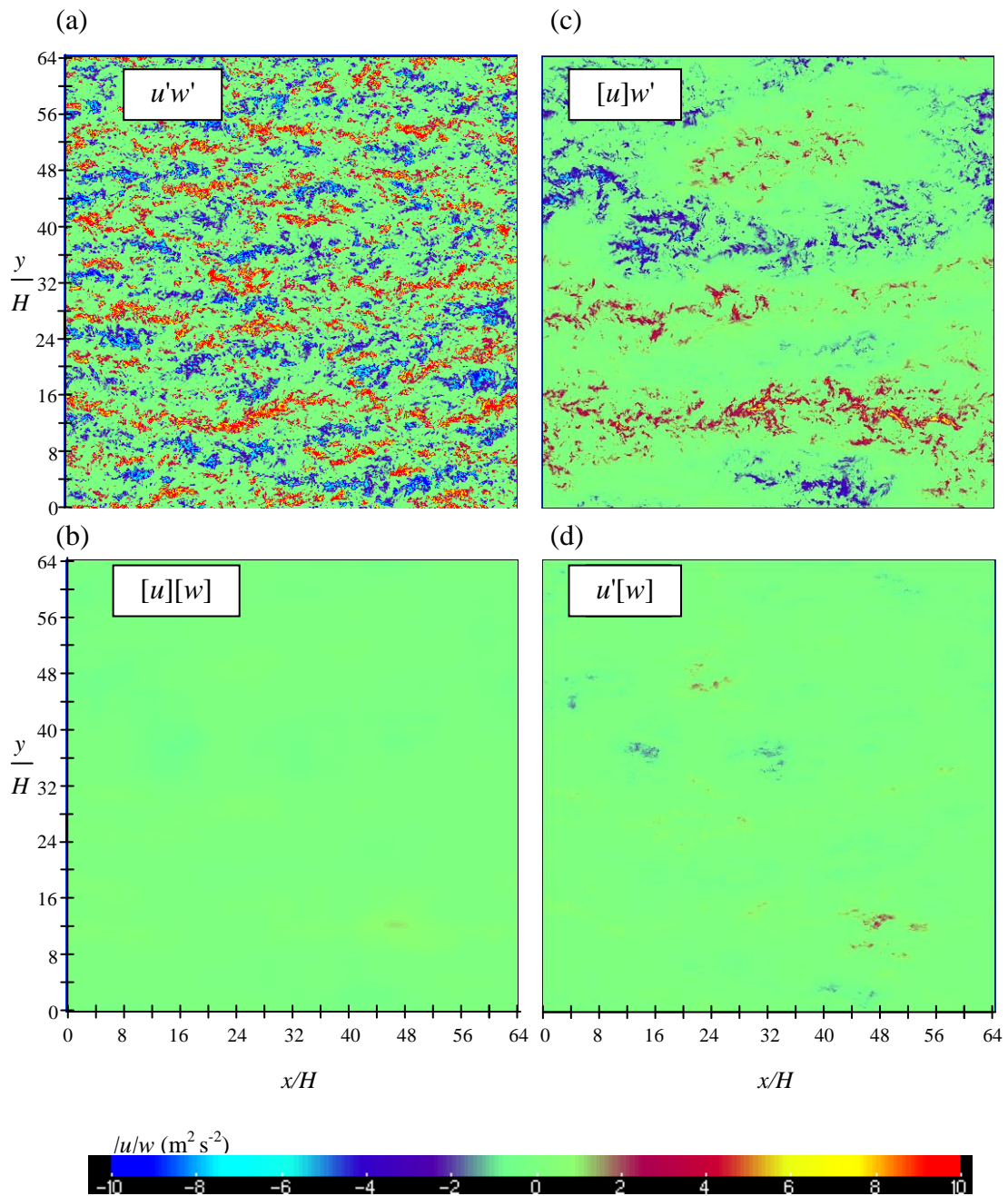


Figure 8. Horizontal instantaneous fields of Reynolds stress components for $z=2H$: (a) covariance of $u'w'$, (b) covariance of $[u][w]$, (c) covariance of $[u]w'$, and (d) covariance of $u'[w]$. The signs of the Reynolds stress components are based on the sign of the vertical component of motion.

distinguish the inner-layer scale motion is the COSMO experiments of Inagaki and Kanda (2010).

The unfiltered values of σ_u/u_* and σ_v/u_* for the large-eddy simulation and COSMO, including the results of the urban experiments (Roth 2000), have large discrepancies. On the other hand, the corresponding linearly-filtered values of σ_u/u_* and σ_v/u_* , plus the results from Cheng and Castro's (2002) wind-tunnel experiments, agree relatively well. The wake component of flow for the wind tunnel, which represents the effects of outer-layer flow, is negligible in the logarithmic layer (Jiménez 2004), which is where spatial decomposition is applied and the extent of the ordinate of Fig. 9. This is evidence for two points: firstly, that filtering method can effectively distinguish the inner-layer motions for an urban atmospheric flow with very high Reynolds number under near-neutral stratification; and secondly, inner-layer turbulence does follow inner-layer scale similarity (Kaimal et al., 1972). Cheng and Castro's (2002) results are closely approximated by the linearly-filtered values since their wind-tunnel experiment is mostly composed of surface-layer motion and the absence of large-scale buoyancy-driven eddies, with a corresponding boundary-layer height set relatively low at $\delta \approx 7.5H$.

In Inagaki and Kanda's (2008, 2010) decomposition of motions, σ_u^2/u_*^2 , σ_v^2/u_*^2 , and σ_w^2/u_*^2 are expressed as:

$$\left(\frac{\sigma_u}{u_*}\right)^2 = \alpha_u + \frac{\langle [u][u] \rangle}{\langle u'w' \rangle} \quad , \quad (13)$$

$$\left(\frac{\sigma_v}{u_*}\right)^2 = \alpha_v + \frac{\langle [v][v] \rangle}{\langle u'w' \rangle} \quad , \quad (14)$$

$$\left(\frac{\sigma_w}{u_*}\right)^2 = \alpha_w \quad , \quad (15)$$

where α_u , α_v , and α_w are constants that express their respective inner-layer scale components. From Fig. 9, these are $\alpha_u \approx (2.0)^2$ and $\alpha_v \approx (1.55)^2$ for the logarithmic layer. Since the vertical component of motion in the logarithmic layer is purely a function of the inner-layer scale, all σ_w/u_* values for $z'/z_o \leq 40$ converge to a value of 1.25, which gives us $\alpha_w \approx (1.25)^2$ for the logarithmic layer. These constants represent the lower limit of the standard deviations σ_u^2/u_*^2 , σ_v^2/u_*^2 , and σ_w^2/u_*^2 (Inagaki and Kanda 2010), and compare well with the observed values in various experiments for urban, flat field, and scale model (Roth 2000, Inagaki and Kanda 2008, 2010).

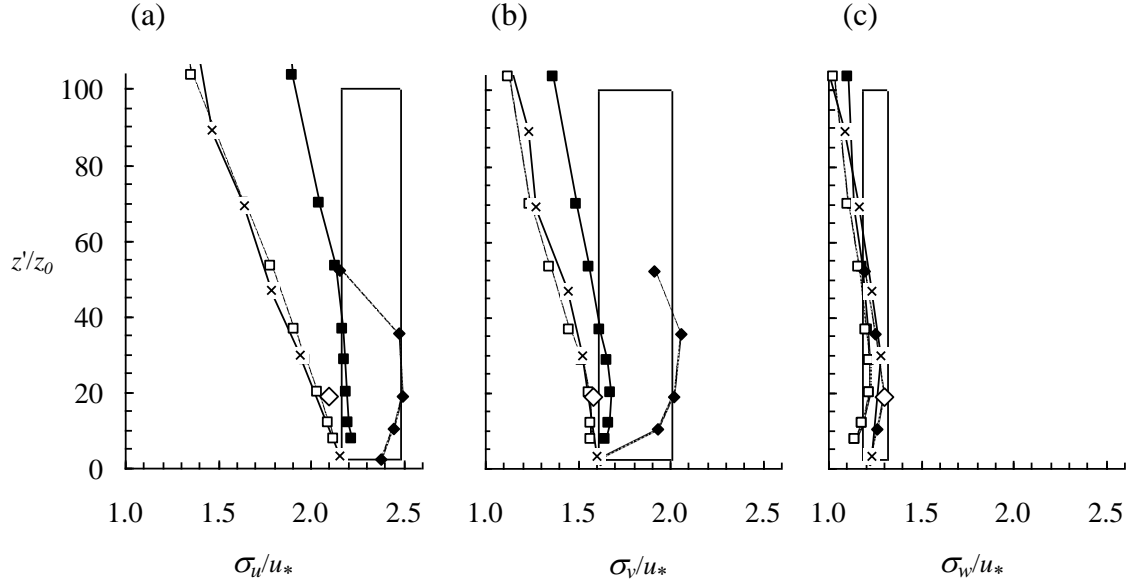


Figure 9. Standard deviations of velocity components, normalised by friction velocity: (a) streamwise component; (b) spanwise component; (c) vertical component. —■— LES, -□- spatially-filtered results of LES, -◆- Inagaki and Kanda (2010), ◇ spatially-filtered results of Inagaki and Kanda (2010), -×- Cheng and Castro (2002), — Roth (2000).

5 Conclusions

A large-eddy simulation of the urban atmospheric boundary layer was performed to investigate the similarity of inner-layer motions and the influence of outer-layer motions at the logarithmic layer, as well as their interaction, wherein the two scales of motions were spatially decomposed. The atmospheric boundary layer is composed of an urban surface layer and a convective mixed layer, and is by far the largest spatial domain ($64H$ by $64H$ by $65H$) with an appropriate resolution ($H/16$) and very high Reynolds numbers ever attempted. Since a horizontal square filter of $10H$ is between the inner-layer scale, $z = 2H$, and the outer-layer scale, $\delta \approx 30H$, and that the inner-layer component of Reynolds stress $\langle u'w' \rangle$ accounts for 95% of the Reynolds stress in the surface layer (i.e., $z = 2H$), the spatial filtering method was able to distinguish between the inner-layer and outer-layer components of turbulence in the inertial sublayer. Close inspection of all the components of the Reynolds stress at $z = 2H$ reveal that the 5% residual on the Reynolds stress is accounted for by the outer-layer scale and interaction terms, negligible relative to the contribution of inner-layer turbulence. From the logarithmic layer, the spatial filter increases with height, wherein the outer-layer eddies gradually take over in turbulence production. Linear filtering along the spanwise direction resulted in a close

approximation of spatial filtering and is more effective in scale separation compared to streamwise-filtering, confirming the results of Inagaki and Kanda (2010).

Similar to Inagaki and Kanda's (2010) intention, the applicability of the MOST to the inner-layer component of horizontal and vertical motions was validated in the large-eddy simulation model as well as with the COSMO experiments. Relative to the horizontal velocity fluctuation u , the inner-layer motions in the surface layer exhibit streaky structures of ejections and sweeps that are more horizontally homogeneous and similar in streamwise scale but smaller in spanwise scale, consistent with the findings of Inagaki and Kanda (2010) in their COSMO experiments. The outer-layer motions, which are large-scale convective rolls in the mixed layer, to some degree influences the location of ejections and sweeps with the updraught and downdraught motions, respectively, thus, disrupting the homogeneity and similarity of the logarithmic layer. The interaction between outer-layer $[u]$ and inner-layer w' motions may be negligible when considering horizontal averages, yet have localised influence on the Reynolds stress that is not insignificant.

References

- R. J. Adrian (2002) Information and the study of turbulence and complex flow. *JSME J Ser B*, 45: 2-8
- Adrian, R. J., Meinhart, C. D., and Tomkins, C. D. (2000) Vortex organization in the outer region of the turbulent boundary layer. *J Fluid Mech* 422: 1-53
- Antonia, R. A. and Rajagopalan, S. (1990) Performance of lateral vorticity probe in a turbulent wake. *Exp Fluids* 9: 118-120
- Antonia, R. A., Raupach, M. R. (1993) Spectral scaling in a high Reynolds number laboratory boundary layer. *Boundary-Layer Meteorol* 65: 289-306
- Bottema, M. (1997) Turbulence closure model "constants" and the problem of "inactive" atmospheric turbulence. *J Wind Eng Ind Aerodyn* 67-68: 897-908
- Bou-Zeid, E., Overney, J., Rogers, B., and Parlange, M. (2009) The effects of building representation and clustering in large eddy simulations of flows in urban canopies. *Boundary-Layer Meteorol* 132: 415-436
- Bradshaw, P. (1967) 'Inactive' motion and pressure fluctuations in turbulent boundary layers. *J Fluid Mech* 30: 241-258
- Businger, J. A., Wyngaard, J. C., Izumi, Y., and Bradley, E. F. (1971) Flux-profile relationships in the atmospheric surface layer. *J Atmos Sci* 28: 181-189
- Castro, I. P., Cheng, H., and Reynolds, R. (2006) Turbulence over urban-type roughness: deductions from wind tunnel measurements. *Boundary-Layer Meteorol* 118: 109-131
- Chakraborty, P., Balachandar, S., and Adrian, R. J. (2005) On the relationships between local vortex identification schemes. *J Fluid Mech* 535: 189-214
- Cheng, H. and Castro, I. P. (2002) Near wall flow over urban-like roughness. *Boundary-Layer Meteorol* 104: 229-259
- Coccali, O., Dobre, A., Thomas, T. G., and Belcher, S. E. (2007) Structure of turbulent flow over regular arrays of cubical roughness. *J Fluid Mech* 589: 375-409
- Deardorff, J. W. (1980) Stratocumulus-capped mixed layers derived from a three-dimensional model. *Boundary-Layer Meteorol* 18: 495-527
- Drobinski, P., Carlotti, P., Newsom, R. K., Banta, R. M., Foster, R. C., and Redelsperger, J.-L. (2004) The structure of the near-neutral atmospheric surface layer. *J Atmos Sci* 61: 699-714
- Dyer, A. J. (1974) A review of flux-profile relationships. *Boundary-Layer Meteorol* 7: 363-372
- Etling, D. and Brown, R. A. (1993) Roll vortices in the planetary boundary layer: a review. *Boundary-Layer Meteorol* 65: 215-248
- Feigenwinter, C., Vogt, R., and Parlow, E. (1999) Vertical structure of selected turbulence characteristics above an urban canopy. *Theor Appl Climatol* 62: 51-63

- Finnigan, J. J. (2000) Turbulence in plant canopies. *Annu Rev Fluid Mech* 32: 519-571
- Finnigan, J. J. and Shaw, R. H. (2000) A wind-tunnel study of airflow in waving wheat: an EOF analysis of the structure of the large-eddy motion. *Boundary-Layer Meteorol* 96: 211-255
- Finnigan, J. J., Shaw, R. H., and Patton, E. G. (2009) Turbulent structure above a vegetation canopy. *J Fluid Mech* 637: 387-424
- Foster, R. C., Vianey, F., Drobinski, P., and Carlotti, P. (2006) Near-surface coherent structures and the vertical momentum flux in a large-eddy simulation of the neutrally-stratified boundary layer. *Boundary-Layer Meteorol* 120: 229-255
- Hagishima, A., Tanimoto, J., Nagayama, K., and Meno, S. (2009) Aerodynamic parameters of regular arrays of rectangular blocks with various geometries. *Boundary-Layer Meteorol* 132: 315-337
- Högström, U. (1988) Non-dimensional wind and temperature profiles in the atmospheric surface layer: a re-evaluation. *Boundary-Layer Meteorol* 42: 55-78
- Högström, U., and Bergström, H. (1996) Organized turbulence structures in the near-neutral surface layer. *J Atmos Sci* 53: 2452-2464
- Högström, U., Hunt, J. C. R., and Smedman, A.-S. (2002) Theory and measurements for turbulence spectra and variances in the atmospheric neutral surface layer. *Boundary-Layer Meteorol* 103: 101-124
- Hunt, J. C. R. and Carlotti, P. (2001) Statistical structure at the wall of the high Reynolds number turbulent boundary layer. *Flow Turb Combust* 66: 453-475
- Hunt, J. C. R. and Morrison, J. F. (2000) Eddy structure in turbulent boundary layers. *Eur J Mech B Fluids* 19: 673-694
- Inagaki, A. (2008) Atmospheric turbulence over an array of massive cubes. Ph.D. dissertation, Tokyo Institute of Technology, Tokyo, 86 pp.
- Inagaki, A. and Kanda, M. (2008) Turbulent flow similarity over an array of cubes in near-neutrally stratified atmospheric flow. *J Fluid Mech* 615: 101-120
- Inagaki, A. and Kanda, M. (2010) Organized structure of active turbulence over an array of cubes within the logarithmic layer of atmospheric flow. *Boundary-Layer Meteorol* 135: 209-228
- Jeong, J. and Hussain, F. (1995) On the identification of a vortex. *J Fluid Mech* 285: 69-94
- Jiménez, J. (1999) The physics of wall turbulence. *Physica A* 263: 252-262
- Jiménez, J. (2004) Turbulent flows over rough walls. *Annu Rev Fluid Mech* 36: 173-196
- Kaimal, J. C. (1978) Horizontal velocity spectra in an unstable surface layer. *J Atmos Sci* 35: 18-24
- Kaimal, J. C. and Finnigan, J. J. (1994) Atmospheric boundary layer flows: their structure and measurement. Oxford University Press, New York, 289 pp.
- Kaimal, J. C., Wyngaard, J. C., Izumi, Y., and Coté, O. R. (1972) Spectral characteristics of surface layer turbulence. *Q J Roy Meteorol Soc* 98: 563-589
- Kanda, M. (2007) Progress in urban meteorology: a review. *J Meteorol Soc Jpn* 85: 363-383
- Kanda M., Moriwaki, R., and Kasamatsu, F. (2004) Large eddy simulation of turbulent organized structure within and above explicitly resolved cube arrays. *Boundary-Layer Meteorol* 112: 343-368
- Kim, K. C. and Adrian, R. J. (1999) Very large-scale motion in the outer layer. *Phys Fluid* 11: 417-422
- Kolář, V. (2007) Vortex identification: new requirements and limitations. *Int J Heat Fluid Flow* 28: 638-652
- Kono, T., Tamura, T., and Ashie, Y. (2010) Numerical investigations of mean winds within canopies of regularly arrayed cubical buildings under neutral stability conditions. *Boundary-Layer Meteorol* 134: 131-155
- Laubach, J. and McNaughton, K. G. (2009) Scaling properties of temperature spectra and heat-flux cospectra in the surface friction layer beneath an unstable outer layer. *Boundary-Layer Meteorol* 133: 219-252
- Letzel, M. O. (2007) High resolution LES of turbulent flow around buildings. Ph.D. dissertation, University of Hannover, Hannover, 126 pp.
- Letzel, M. O., Krane, M., and Raasch, S. (2008) High resolution urban large-eddy simulation studies from street canyon to neighborhood scale. *Atmos Envi* 42: 8770-8784
- Mahrt, L., and Gibson, W. (1992) Flux decomposition into coherent structures. *Boundary-Layer Meteorol* 60: 143-168
- Maitani, T., and Shaw, R. H. (1990) Joint probability analysis of momentum and heat fluxes at a deciduous forest. *Boundary-Layer Meteorol* 52: 283-300
- McNaughton, K. G. (2004) Turbulence structure of the unstable atmospheric surface layer and transition to the outer layer. *Boundary-Layer Meteorol* 112: 199-221
- McNaughton, K. G. (2006) On the kinetic energy budget of the unstable atmospheric surface layer. *Boundary-Layer Meteorol* 118: 83-107
- McNaughton, K. G., and Brunet Y. (2002) Townsend's hypothesis, coherent structures and Monin-Obukhov similarity. *Boundary-Layer Meteorol* 102: 161-175
- McNaughton, K. G., and Laubach, J. (1998) Unsteadiness as a cause of non-equality of eddy diffusivities for heat and vapour at the base of an advective inversion. *Boundary-Layer Meteorol* 88: 479-504
- McNaughton, K. G. and Laubach, J. (2000) Power spectra and cospectra for wind and scalars in a disturbed surface layer at the base of an advective inversion. *Boundary-Layer Meteorol* 96: 143-185
- Moeng, C.-H. and Sullivan, P. P. (1994) A comparison of shear- and buoyancy-driven planetary boundary layer flows. *J Atmos Sci* 51: 999-1022
- Monin, A. S. and Obukhov, A. M. (1954) Basic laws of turbulent mixing in the surface layer of the atmosphere. *Tr Akad Nauk SSSR Geofiz Inst* 24, 163-187. English translation by John Miller, 1959

- Morrison, J. F. (2007) The interaction between inner and outer regions of turbulent wall-bounded flow. *Phil Trans Roy Soc A* 365: 683-698
- Morrison, J. F., Jiang, W., McKeon, B. J., and Smits, A. J. (2002) Reynolds number dependence of streamwise velocity spectra in turbulent pipe flow. *Phys Rev Lett* 88: 214501
- Poggi, D. and Katul, G. (2008) Turbulent intensities and velocity spectra for bare and forested gentle hills: flume experiments. *Boundary-Layer Meteorol* 129: 25-46
- Raasch, S. and Schröter, S. (2001) A large-eddy simulation model performing on massively parallel computers. *Meteorol Z* 10: 363-372
- Raupach, M. R. (1981) Conditional statistics of Reynolds stress in rough-wall and smooth-wall turbulent boundary layers. *J Fluid Mech* 108: 363-382
- Raupach, M. R., Antonia, R. A., and Rajagopalan, S. (1991) Rough-wall turbulent boundary layers. *Appl Mech Rev* 44: 1-25
- Raupach, M. R., Finnigan, J. J., and Brunet, Y. (1996) Coherent eddies and turbulence in vegetation canopies: the mixing-layer analogy. *Boundary-Layer Meteorol* 78: 351-382
- Richardson, L. F., (1920) The supply of energy from and to atmospheric eddies. *Proc Roy Soc Lond A* 97: 354-373
- Robinson, S. K. (1991) Coherent motions in the turbulent boundary layer. *Annu Rev Fluid Mech* 23: 601-639
- Rotach, M. W. (1993) Turbulence close to a rough urban surface part II: Variances and gradients. *Boundary-Layer Meteorol* 66: 75-92
- Rotach M. W., Vogt, R., Bernhofer, C., Batchvarova, E., Christen, A., Clappier, A., Feddersen, B., Gryning, S.-E., Martucci, G., Mayer, H., Mitev, V., Oke, T. R., Parlow, E., Richner, H., Roth, M., Roulet, Y.-A., Ruffieux, D., Salmond, J. A., Schatzmann, M., and Vogt, J. A. (2005) BUBBLE – an urban boundary layer meteorology project. *Theor Appl Climatol* 81: 231-261
- Roth, M. (2000) Review of atmospheric turbulence over cities. *Q J Roy Meteorol Soc* 126: 941-990
- Shaw, R. H., Brunet, Y., Finnigan, J. J., and Raupach, M. R. (1995) A wind tunnel study of air flow in waving wheat: Two-point velocity statistics. *Boundary-Layer Meteorol* 76: 349-376
- Shaw, R. H., Tavanger, J., and Ward, D. P. (1983) Structure of the Reynolds stress in a canopy layer. *J Clim Appl Meteorol* 22: 1922-1931
- Stull, R. B. (1988) *An introduction to boundary layer meteorology*. Kluwer Academic Press, The Netherlands, 680 pp.
- Su, H.-B., Shaw, R. H., U, K. P., Moeng, C.-H., and Sullivan, P. P. (1998) Turbulent statistics of neutrally stratified flow within and above a sparse forest from large-eddy simulation and field observations. *Boundary-Layer Meteorol* 88: 363-397
- Townsend, A. A. (1961) Equilibrium layers and wall turbulence. *J Fluid Mech* 11: 97-120
- Townsend, A. A. (1976) *The structure of turbulent shear flow*. Cambridge University Press, Cambridge, 315 pp.
- Van Gorsel, E., Christen, A., Feigenwinter, C., Parlow, E., and Vogt, R. (2003) Daytime turbulence statistics above a steep forested slope. *Boundary-Layer Meteorol* 109: 311-329
- Wallace, J. M., Eckelmann, H., and Brodkey, R. S. (1972) The wall region in turbulent shear flow. *J Fluid Mech* 54: 39-48
- Willmarth, W. W., and Lu, S. S. (1972) Structure of the Reynolds stress near the wall. *J Fluid Mech* 55: 65-92
- Wyngaard, J. C. and Coté, O.R. (1971) The budgets of turbulent kinetic energy and temperature variance in the atmospheric surface layer. *J Atmos Sci* 28: 190-201
- Xie, Z.-T., Coceal, O. And Castro, I. P. (2008) Large-eddy simulation of flows over random urban-like obstacles. *Boundary-Layer Meteorol* 129: 1-23
- Zhao, R. and Smits, A. J. (2007) Wall-normal turbulence statistics in high Reynolds number flow. *J Fluid Mech* 576: 457-473